



Article

Insight into Unsteady Separated Stagnation Point Flow of Hybrid Nanofluids Subjected to an Electro-Magneto hydrodynamics Riga Plate

Najiyah Safwa Khashi'ie ¹, Norihan Md Arifin ^{2,3,*}, Nur Syahirah Wahid ³ and Ioan Pop ⁴

¹ Fakulti Teknologi Kejuruteraan Mekanikal dan Pembuatan, Universiti Teknikal Malaysia Melaka, Hang Tuah Jaya, Durian Tunggal, Melaka 76100, Malaysia

² Institute for Mathematical Research, Universiti Putra Malaysia, UPM Serdang, Serdang 43400, Malaysia

³ Department of Mathematics, Faculty of Science, Universiti Putra Malaysia, UPM Serdang, Serdang 43400, Malaysia

⁴ Department of Mathematics, Babeş-Bolyai University, 400084 Cluj-Napoca, Romania

* Correspondence: norihana@upm.edu.my

Abstract: The main objective of this work is to analyze and compare the numerical solutions of an unsteady separated stagnation point flow due to a Riga plate using copper–alumina/water and graphene–alumina/water hybrid nanofluids. The Riga plate generates electro-magneto hydrodynamics (EMHD) which is expected to delay the boundary layer separation. The flow and energy equations are mathematically developed based on the boundary layer assumptions. These equations are then simplified with the aid of the similarity variables. The numerical results are generated by the *bvp4c* function and then presented in graphs and tables. The limitation of this model is the use of a Riga plate as the testing surface and water as the base fluid. The results may differ if another wall surfaces or base fluids are considered. Another limitation is the Takabi and Salehi's correlation of hybrid nanofluid is used for the computational part. The findings reveal that dual solutions exist where the first solution is stable using the validation from stability analysis. Graphene–alumina/water has the maximum skin friction coefficient while copper–alumina/water has the maximum thermal coefficient for larger acceleration parameter. Besides, the single nanofluids (copper–water, graphene–water and alumina–water) are also tested and compared with the hybrid nanofluids. Surprisingly, graphene–water has the maximum skin friction coefficient while alumina–water has the maximum heat transfer rate. The findings are only conclusive and limited to the comparison between graphene–alumina and copper–alumina with water base fluid. The result may differ if another base fluid is used. Hence, future study is necessary to investigate the thermal progress of these hybrid nanofluids.

Keywords: electro-magneto hydrodynamics; heat transfer; hybrid nanofluid; separated stagnation; stability analysis; unsteady flow



Citation: Khashi'ie, N.S.; Arifin, N.M.; Wahid, N.S.; Pop, I. Insight into Unsteady Separated Stagnation Point Flow of Hybrid Nanofluids Subjected to an Electro-Magneto hydrodynamics Riga Plate. *Magnetochemistry* **2023**, *9*, 46. <https://doi.org/10.3390/magnetochemistry9020046>

Academic Editors: Devashibhai Adroja, Dmitry Alexandrovich Filippov and Carlos J. Gómez García

Received: 4 December 2022

Revised: 5 January 2023

Accepted: 29 January 2023

Published: 31 January 2023



Copyright: © 2023 by the authors. Licensee MDPI, Basel, Switzerland. This article is an open access article distributed under the terms and conditions of the Creative Commons Attribution (CC BY) license (<https://creativecommons.org/licenses/by/4.0/>).

1. Introduction

Over the course of many decades, the amount of research that has been carried out to improve the thermal efficiency of industrial equipment has steadily increased. A variety of active and passive techniques have been developed by researchers to improve the thermal performance of a system. One of the most well-known techniques is by employing the smart heat transfer fluid known as nanofluid. Nanofluid is produced by dispersing a small amount of nanosized particles either metallic or non-metallic (e.g., copper, alumina, silver, magnetite, cobalt ferrite) into a carrier fluid like water, oil, ethylene glycol, etc. (see Choi and Eastman [1]). Multiple investigations have shown that even at low concentrations, nanoparticles possess special features in terms of thermal performance, particularly enhancements in thermal conductivity [2]. The special properties of nanofluid

have been scrutinized comprehensively by Yu et al. [3], Yu and Xie [4], Das et al. [5], and Ali and Salam [6].

After the development of nanofluid, recently, researchers have found another new heat transfer fluid which considers two different kinds of nanoparticles. The thermal conductivity of hybrid nanofluid is higher than that of conventional nanofluid, enabling it to be useful in a wide range of thermal transmission applications like heat pipes, solar collectors and heat exchangers [7–11]. On the other hand, far more research must be carried out on hybrid nanofluid in order to make the most of its unique qualities. In this context, a significant amount of experimental research pertaining to hybrid nanofluids has been carried out. For instance, Suresh et al. [12] experimented a laminar convective heat transfer and pressure drop properties of hybrid nanofluid via a heated circular tube. Their findings presented that the hybrid nanofluid creates a higher Nusselt number compared to the regular base fluid. Madhesh and Kalaiselvam [13] also stated that the heat transfer rate was found to be maximum for hybrid nanofluid in their experimental study. Additionally, the heat transfer of hybrid nanofluid has been proven to enhance when the concentration of nanoparticles is maximized accordingly (see Alawi et al. [14]).

The Riga plate was one of the most notable breakthroughs for overcoming weak fluid conductivity (see Gailitis and Lielausis [15]). This device is an electromagnetic actuator that is made up of alternating pairs of electrodes and magnets. It is used to generate an electromagnetic field that produced the Lorentz force to regulate the fluid flow. Besides, the Riga plate can be used to minimize surface friction and prevent turbulence formation [16]. Upon reviewing the literature, the flow of nanofluid over a Riga plate has been previously carried out by Hayat et al. [17]. Ayub et al. [18] examine the magnetic slip flow of a viscous nanofluid across a Riga plate. Ramzan et al. [19] then also considered the heated Riga plate towards the radiative Williamson nanofluid with the combination of a chemical reaction. Due to the concern towards the heat transfer advancement, hybrid nanofluid has also been considered by the researchers to interrogate its properties when the flow is configured over a Riga plate. Zari et al. [20] analyzed the radiative Hiemenz flow of copper–alumina/water nanofluid towards an EMHD Riga plate. Some of the recent works are contributed by Abbas et al. [21], Khashi'ie et al. [22–24], Zainal et al. [25], Wahid et al. [26], Tabassum et al. [27], Shatnawi et al. [28], Siddique et al. [29], Kumar [30] and Asogwa et al. [31].

The stagnation point flow occurs when an inviscid and outer flow impinges on a solid surface (fixed or moving) with a certain strain rate. This flow phenomenon is seen to be steady if the strain rate remains the same throughout time, whereas the unsteady flow is supposed to be the opposite of steady flow. When it comes to engineering processes, steady flow is preferred since it makes operations much easier to control. Engineers also find it easier to predict the outcomes of such processes. However, real-world experience demonstrates that even in the ideal scenario of fluid flow, undesired unstable effects may still manifest themselves in close proximity to a device. These undesirable consequences might be the result of self-inflicted motions of the body or non-uniformities in the fluid. Both of these possibilities are possible. The unsteady separated stagnation point (USSP) flow in a two-dimensional system due to an impermeable surface has been studied by Ma and Hui [32]. Then, Dholey and Gupta [33,34] improved the flow problem by considering the transpiration effect. Lok and Pop [35] considered the similar problem by considering the stretched/shrunk surface. Later, Dholey [36–38] inserted magnetohydrodynamic (MHD) effect towards the USSP flow problem, while Roşca et al. [39], Renuka et al. [40], Khashi'ie et al. [41], and Zainal et al. [42] integrated it with the hybrid nanofluid model.

Upon a thorough exploration of the relevant literature, it is found that only limited studies have been conducted regarding the USSP flow of a hybrid nanofluid driven by a Riga plate. Thus, it is interesting and important to investigate such problems as it can be useful for future guidance in the area of fluid dynamics. In this study, we provide the formulation of the model together with the numerical solutions under a possible specific configuration. The governing mathematical equations of the flow model are simplified using the relevant similarity transformations, and then are solved using *bvp4c* (Matlab).

In addition, stability analysis is provided so that the features of the numerical solutions may be investigated. Using the control parameters that were taken into consideration, this research might give insight and guidance that could be used to correctly regulate the flow mechanism of a hybrid nanofluid.

2. Mathematical Formulation

The unsteady separated stagnation point flow of two hybrid nanofluids (copper–alumina/water and graphene–alumina/water) as depicted in Figure 1 are analyzed subjected to a moving plate with few physical assumptions as stated below:

- The term $\frac{\pi j_0 M_1}{8\rho_{hnf}} \exp(-\pi y_1/p)$ in the mathematical model is used to represent the electro-magneto-hydrodynamics effect from the Riga plate where $M_1 = \frac{M_0(x-x_0(t))}{(t_{ref}-\beta t)^2}$ and $y_1 = y/\sqrt{t_{ref}-\beta t}$; j_0 is the electrodes' current density, M_0 is a constant, t_{ref} is the reference time (constant), p is the width of magnets and electrodes, β is the unsteadiness accelerating/decelerating parameter, t is the time and $x_0(t)$ is the plate's displacement.
- The velocity of free stream flow which align with the plate is $u_e(x,t) = \alpha \frac{(x-x_0(t))}{t_{ref}-\beta t} + u_0(t)$; α is the acceleration parameter. Meanwhile, the velocity of the moving plate is $u_0(t) = \partial x_0(t)/\partial t$.
- The terms T_w and T_∞ respectively stand for surface and ambient temperatures.
- The sedimentation and aggregation effects are omitted by considering that the nanofluids are stable.

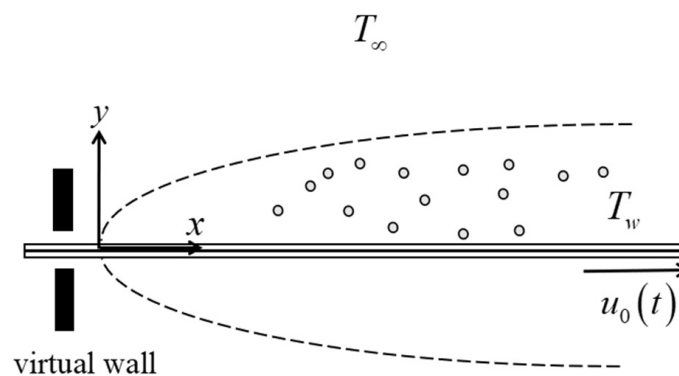


Figure 1. Illustration of the physical model.

The modelling equations subjected to the above stated model are (see Dholey [36] and Khashi'ie et al. [43])

$$\frac{\partial u}{\partial x} + \frac{\partial v}{\partial y} = 0, \tag{1}$$

$$\frac{\partial u}{\partial t} + u \frac{\partial u}{\partial x} + v \frac{\partial u}{\partial y} = \frac{\partial u_e}{\partial t} + u_e \frac{\partial u_e}{\partial x} + \frac{\mu_{hnf}}{\rho_{hnf}} \frac{\partial^2 u}{\partial y^2} + \frac{\pi j_0 M_1}{8\rho_{hnf}} \exp(-\pi y_1/p), \tag{2}$$

$$\frac{\partial T}{\partial t} + u \frac{\partial T}{\partial x} + v \frac{\partial T}{\partial y} = \frac{k_{hnf}}{(\rho C_p)_{hnf}} \frac{\partial^2 T}{\partial y^2}, \tag{3}$$

$$\begin{aligned} u = u_0, v = 0, T = T_w \text{ at } y = 0 \\ u \rightarrow u_e, T \rightarrow T_\infty \text{ as } y \rightarrow \infty \end{aligned} \tag{4}$$

The similarity transformation which is useful to simplify the complex model is [36,43]

$$u = \alpha \frac{x - x_0}{t_{ref} - \beta t} f'(\eta) + u_0, v = -\alpha \sqrt{\frac{\nu_f}{t_{ref} - \beta t}} f(\eta), \theta(\eta) = \frac{T - T_\infty}{T_w - T_\infty}, \eta = \frac{y}{\sqrt{\nu_f (t_{ref} - \beta t)}}. \tag{5}$$

The transformed equations (ODEs) and reduced boundary conditions (BCs) are obtained upon the substitution of similarity transformation which is useful to simplify the similarity transformation which useful to simplify the Equation (5) into Equations (2)–(4).

$$\frac{\mu_{hnf}/\mu_f}{\rho_{hnf}/\rho_f} f''' + \alpha (ff'' - f'^2 + 1) - \beta(0.5\eta f'' + f' - 1) + \frac{Z}{\rho_{hnf}/\rho_f} \exp(-d\eta) = 0, \tag{6}$$

$$\frac{k_{hnf}/k_f}{Pr(\rho C_p)_{hnf}/(\rho C_p)_f} \theta'' + \alpha f\theta' - 0.5\beta\eta\theta' = 0, \tag{7}$$

$$f(0) = 0, f'(0) = 0, \theta(0) = 1, f'(\infty) \rightarrow 1, \theta(\infty) \rightarrow 0, \tag{8}$$

From Equations (6) and (7), $d = \frac{\pi\sqrt{\nu_f}}{p}$ is the width parameter, $Z = \frac{\pi j_0 M_0}{8a\rho_f}$ is the EMHD parameter and $Pr = (\mu C_p)_f/k_f$ is the Prandtl number. The properties for the nanoparticles and water base fluid are listed in Table 1. Meanwhile, the correlations of hybrid nanofluid’s properties are shown in Table 2 (see Takabi and Salehi [44]).

Table 1. Physical properties.

Properties	Water	Copper	Graphene	Alumina
ρ (kg/m ³)	997.1	8933	2200	3970
C_p (J/kgK)	4179	385	790	765
k (W/mK)	0.613	400	5000	40

Table 2. General correlations of hybrid nanofluids.

Properties	Correlations
Thermal conductivity	$k_{hnf} = \left[\frac{\left(\frac{\phi_1 k_1 + \phi_2 k_2}{\phi_{hnf}}\right) - 2\phi_{hnf} k_f + 2(\phi_1 k_1 + \phi_2 k_2) + 2k_f}{\left(\frac{\phi_1 k_1 + \phi_2 k_2}{\phi_{hnf}}\right) + \phi_{hnf} k_f - (\phi_1 k_1 + \phi_2 k_2) + 2k_f} \right] k_f$
Heat capacity	$(\rho C_p)_{hnf} = \phi_1 (\rho C_p)_{s1} + \phi_2 (\rho C_p)_{s2} + (1 - \phi_{hnf}) (\rho C_p)_f$
Density	$\rho_{hnf} = \phi_1 \rho_{s1} + \phi_2 \rho_{s2} + (1 - \phi_{hnf}) \rho_f$
Dynamic viscosity	$\mu_{hnf} = \frac{\mu_f}{(1 - \phi_{hnf})^{2.5}}; \phi_{hnf} = \phi_1 + \phi_2$

The similarity transformation method as presented in Equation (5) is the common method for the nondimensionalization process of the boundary layer equations so that it can be easily solved using the bvp4c solver or other numerical approaches. From the similarity technique, the boundary layer and energy equations are transformed into a set of ordinary differential equations which are simpler to solve. However, depending on the physical situations and restrictions, similarity technique is not suitable. Hence, a few methods have been introduced to solve the original model in partial differential equations, for example method of local non-similarity (LNS) as introduced by Sparrow and Yu [45] and also discussed by Hussain and Sheremet [46]. Meanwhile, Kumar et al. [47] used the Laplace and Hankel transformations to analyze the general solution of two dimensional incompressible and axisymmetric fluid flow through porous media. The combination of Laplace transform with eigenvalue technique was also adopted by Abbas [48] for the solution of thermoelastic diffusion in an infinite medium with a spherical cavity.

3. Stability Analysis

The stability analysis is performed upon the observation of multiple solutions. The transformation with the inclusion of time variable is introduced as follows [49]:

$$\left. \begin{aligned} \tau &= \frac{\alpha t}{t_{ref} - \beta t}, u = \alpha \frac{x - x_0(t)}{t_{ref} - \beta t} \frac{\partial f(\eta, \tau)}{\partial \eta} + u_0(t), v = -\alpha \sqrt{\frac{\nu_f}{t_{ref} - \beta t}} f(\eta, \tau), \\ \theta(\eta, \tau) &= \frac{T - T_\infty}{T_w - T_\infty}, \eta = \frac{y}{\sqrt{\nu_f(t_{ref} - \beta t)}}. \end{aligned} \right\} \quad (9)$$

By substituting Equation (9) into Equations (2)–(4), the reduced equations are

$$\frac{\mu_{hnf}/\mu_f}{\rho_{hnf}/\rho_f} \frac{\partial^3 f}{\partial \eta^3} + \alpha \left(f \frac{\partial^2 f}{\partial \eta^2} - \frac{\partial f}{\partial \eta} \frac{\partial f}{\partial \eta} + 1 \right) - \beta \left(0.5\eta \frac{\partial^2 f}{\partial \eta^2} + \frac{\partial f}{\partial \eta} - 1 \right) + \frac{Z}{\rho_{hnf}/\rho_f} \exp(-d\eta) - \alpha(1 + \beta\tau) \frac{\partial^2 f}{\partial \eta \partial \tau} = 0, \quad (10)$$

$$\frac{k_{hnf}/k_f}{Pr(\rho C_p)_{hnf}/(\rho C_p)_f} \frac{\partial^2 \theta}{\partial \eta^2} + \alpha f \frac{\partial \theta}{\partial \eta} - 0.5\beta\eta \frac{\partial \theta}{\partial \eta} - \alpha(1 + \beta\tau) \frac{\partial \theta}{\partial \tau} = 0, \quad (11)$$

$$f(0, \tau) = 0, \frac{\partial f}{\partial \eta}(0, \tau) = 0, \theta(0, \tau) = 1, \frac{\partial f}{\partial \eta}(\infty, \tau) \rightarrow 1, \theta(\infty, \tau) \rightarrow 0 \quad (12)$$

The reduced equations and condition in Equations (10)–(12) are then tested using eigenvalue approach for any possible disturbance. The perturbation equations are [50]:

$$\begin{aligned} f(\eta, \tau) &= f_0(\eta) + e^{-\gamma\tau} F(\eta, \tau), \\ \theta(\eta, \tau) &= \theta_0(\eta) + e^{-\gamma\tau} G(\eta, \tau). \end{aligned} \quad (13)$$

By substituting Equation (13) into Equations (10)–(12), the linearized set of eigenvalue equations are obtained with the consideration of a relaxing boundary condition as suggested by Harris et al. [51].

$$\frac{\mu_{hnf}/\mu_f}{\rho_{hnf}/\rho_f} F''' + \alpha(f_0 F'' + F f_0'' - 2f_0' F') - \beta(0.5\eta F'' + F') + \alpha\gamma F' = 0, \quad (14)$$

$$\frac{k_{hnf}/k_f}{Pr(\rho C_p)_{hnf}/(\rho C_p)_f} G'' + \alpha(f_0 G' + F\theta_0') - 0.5\beta\eta G' + \alpha\gamma G = 0, \quad (15)$$

$$\begin{aligned} F(0) &= 0, F'(0) = 0, F''(0) = 0 \text{ (replaced)}, G(0) = 0, \\ F'(\eta) &\rightarrow 0 \text{ (relaxed)}, G(\eta) \rightarrow 0 \text{ as } \eta \rightarrow \infty. \end{aligned} \quad (16)$$

For the successful smallest eigenvalues, $F'_0(\eta) \rightarrow 0$ as $\eta \rightarrow \infty$ is substituted with $F''(0) = 1$.

4. Results and Discussion

The numerical computation is fully conducted using the bvp4c application in the Matlab software by first reducing Equations (6)–(8) into the coded equation. The results are displayed for the variations of (a) skin friction coefficient, (b) heat transfer/thermal rate, (c) velocity, and (d) temperature of the tested working fluids (copper–alumina/water and graphene–alumina/water). Besides, the results are portrayed to highlight the effects of pertinent parameters like EMHD parameter Z and acceleration parameter α towards the unsteadiness parameter β with fixed volumetric nanoparticle's concentration $\phi_1, \phi_2 = 0.01$, Prandtl number $Pr = 6.2$ and width parameter $d = 0.01$. Table 3 shows the comparison of numerical values with previous results for the validation purpose. The present value (1.5394731) is consistent with the other values yet shows the accuracy of the present model. Meanwhile, Table 4 presents the smallest eigenvalues by solving the Equations (14)–(16) using the bvp4c application. Positive values of γ_1 denote that the solution is stable. Another

way to check if the stability analysis is correct by observing the trend of γ_1 where $\gamma_1 \rightarrow 0$ as $\beta \rightarrow \beta_c$.

Table 3. Validation when $Z = d = 0.5$, $\phi_1 = \phi_2 = 0$ and $\alpha = 1$ with previous findings.

$f''(0)$	Present	Khashi'ie et al. [43]	Ahmad et al. [52]
	1.5394731	1.5394680	1.5394682

Table 4. Smallest eigenvalue for the stability analysis of the graphene–alumina/water when $\phi_1 = \phi_2 = Z = d = 0.01$ and $\alpha = 1$.

β	γ_1	
	First Solution	Second Solution
−5.03	0.0487	−0.0486
−5.031	0.0312	−0.0311
−5.0315	0.0165	−0.0165
−5.0316	0.0115	−0.0115
−5.0318	0.0025	−0.0041

The USSP flow of the working fluids usually can produce dual solutions based on the unsteadiness strength. The unsteadiness parameter measures three cases: accelerating case for $\beta > 0$, decelerating case for $\beta < 0$ and steady state case when $\beta = 0$. Dual solutions normally appear when $\beta < 0$ by virtue of the boundary layer thickening from the instability of the vortices. These dual solutions are available up to a critical value or the end point of the boundary layer solutions as demonstrated in Figures 2–4. Another subject of interest for the USSP flow is the separation value between AFS-attached flow solution ($f''(0) > 0$) and RFS-reverse flow solution ($f''(0) < 0$). Usually, the AFS is only possible up to a certain value of the unsteadiness parameter and it is possible when $\beta < 0$. However, the priority of this work is to observe the flow and thermal characteristics of the nanofluids when high magnitude of negative β is considered.

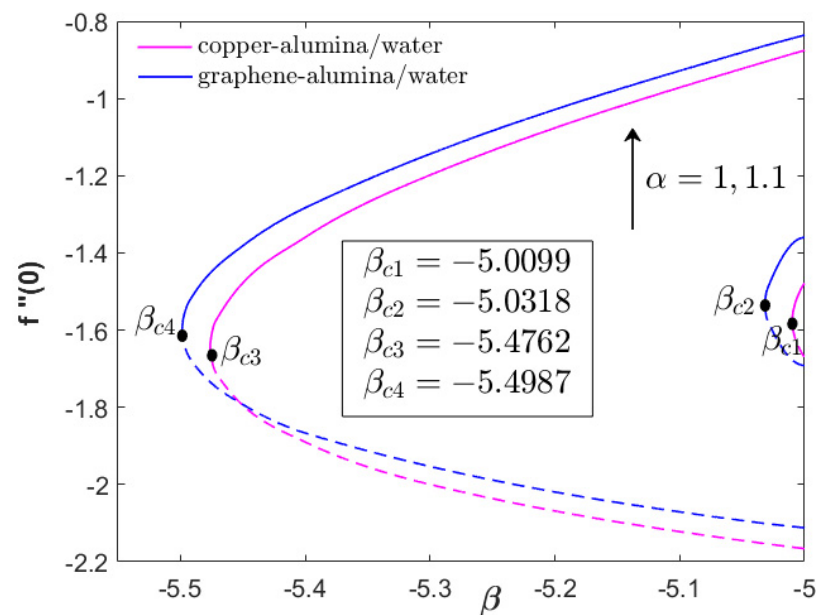


Figure 2. $f''(0)$ for various hybrid nanofluids and α (acceleration parameter) when $\phi_1 = \phi_2 = 0.01$ and $Z = d = 0.01$.

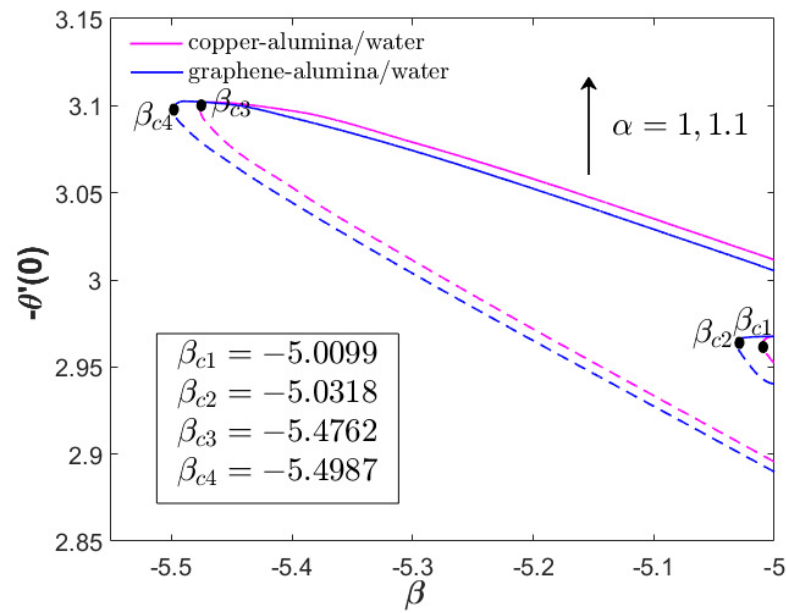


Figure 3. $-\theta'(0)$ for various hybrid nanofluids and α (acceleration parameter) when $\phi_1 = \phi_2 = 0.01$ and $Z = d = 0.01$.

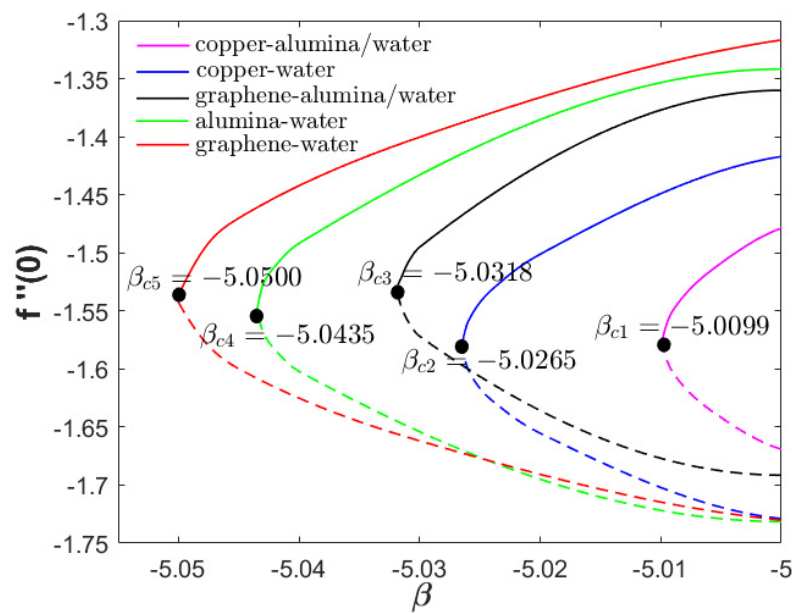


Figure 4. $f''(0)$ for various working fluids when $\alpha = 1$ and $Z = d = 0.01$.

Figures 2 and 3 compare $f''(0)$ and $-\theta'(0)$ of the copper–alumina/water and graphene–alumina water hybrid nanofluids when $\alpha = 1$ (basic Hiemenz flow) and $\alpha = 1.1$. In Figure 2, the negative values of $f''(0)$ for both hybrid nanofluids within the range of unsteadiness parameter $\beta_c \leq \beta \leq -5$ implies that the solutions are reverse flow solutions (RFS). Few studies have highlighted the observation of attached flow solution (AFS) when $\beta < 0$ and $\beta > 0$. However, no AFS ($f''(0) > 0$) is seen in Figure 2 due to the high magnitude of unsteadiness decelerating parameter which tends to weaken the vortices of the fluid flow (see). In addition, as the decelerating parameter increases $\beta \rightarrow \beta_c$, the value of $f''(0)$ slightly decreases for both hybrid nanofluids which shows the retardation of the fluid flow. However, upon the increment of the acceleration parameter ($\alpha = 1, 1.1$), the value of $f''(0)$ significantly increases due the role of the acceleration parameter in stabilizing the vortices and enhancing the flow progress. From Figure 2, it is obvious that the graphene–alumina/water

has higher skin friction and critical value ($\beta_c = -5.0318$ ($\alpha = 1$), $\beta_c = -5.4987$ ($\alpha = 1.1$)) than the copper–alumina/water ($\beta_c = -5.0099$ ($\alpha = 1$), $\beta_c = -5.4762$ ($\alpha = 1.1$)) which indicates that the combination of graphene and alumina nanoparticles is progressive in assisting the fluid movement and delaying the boundary layer separation. Moreover, from Figure 3, the heat transfer coefficient of the copper–alumina/water is moderately greater than the graphene–alumina/water within a certain range of the decelerating parameter. However, the graphene–alumina/water is still the best option for the heat transfer fluid as we can see that the value of $-\theta'(0)$ is the greatest when considering maximum decelerating parameter ($\beta_c = -5.4987$).

Figures 4 and 5 compares the distributions of $f''(0)$ and $-\theta'(0)$ for different working nanofluids (hybrid and single) namely copper–alumina/water, graphene–alumina/water, copper–water, graphene–water and alumina–water. The graphene–water (nanofluid) has the maximum skin friction coefficient and critical value followed by alumina–water (nanofluid), graphene–alumina/water (hybrid nanofluid), copper–water (nanofluid) and copper–alumina/water (hybrid nanofluid) as depicted in Figure 4. Surprisingly, in Figure 5, the nanofluids have greater thermal rate than the hybrid nanofluids such that alumina–water > graphene–water > copper–water > graphene–alumina/water > copper–alumina/water. This outcome is supported by the experimental findings by Ahammed et al. [53] such that the graphene–water nanofluid augmented the heat transfer coefficient for the heat exchanger application up to 88.62% followed by graphene–alumina/water hybrid nanofluid (63.13%) and alumina–water nanofluid (31.89%), respectively.

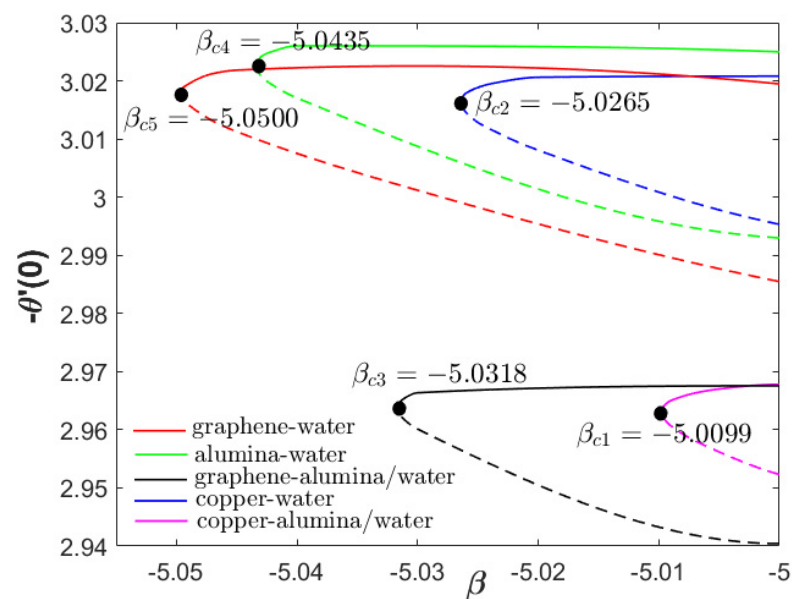


Figure 5. $-\theta'(0)$ for various working fluids when $\alpha = 1$ and $Z = d = 0.01$.

Figures 6–9 present the velocity and temperature of the graphene–alumina water hybrid nanofluid with different testing parameters (unsteadiness decelerating parameter, EMHD parameter and width parameter). All the profiles comply with the boundary condition (8), hence fulfill the validation criteria of the pertinent model. Similar to the previous figures, Figures 6–9 also portray the potential second solution. Previous studies have shown that the USSP flow could produce two solutions with the first solution as the real one. In Figure 6, the first/physical solution for the velocity profile decreases as the decelerating parameter enhances which contradicts the second solution. Meanwhile, both solutions for the temperature profile reduces with the increment of β . Physically, the addition of β leads to higher resistance in fluid movement and consequently, reduces the velocity profile. In Figure 7, the temperature profile also depreciates due to the active heat transport from the hot fluid to the cool ambient. The effect of EMHD parameter (generated

from the Riga plate) on the flow and thermal profiles is displayed in Figures 8 and 9. The velocity of the hybrid nanofluid enhances while the temperature profile lessens with the increment of Z . The EMHD effect physically can assist the fluid movement by reducing the wall drag which, consequently, accelerates the fluid velocity whilst delays the separation of laminar flow. Meanwhile, the reduction in the temperature profile is consistent with the active process of the heat transfer transmission.

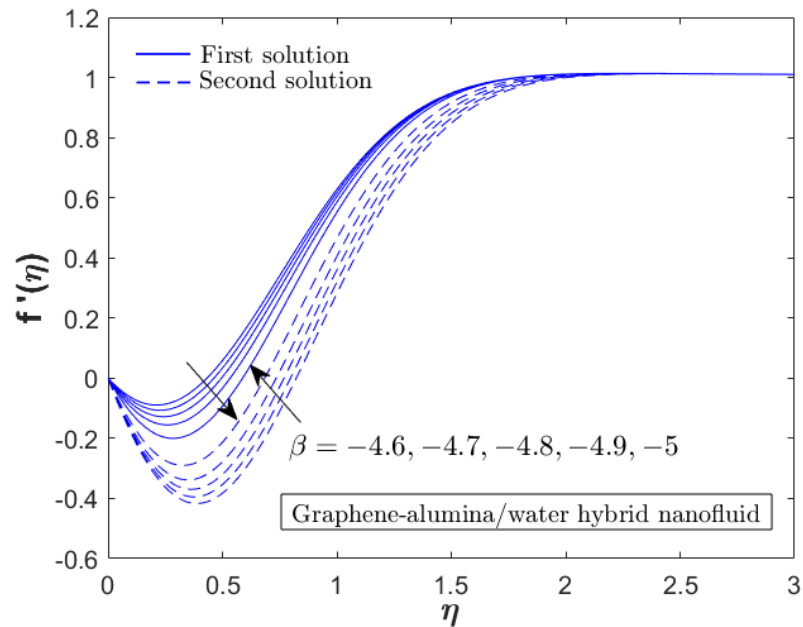


Figure 6. Velocity profile for various β (decelerating parameter) when $\alpha = 1$ and $Z = d = \phi_1 = \phi_2 = 0.01$.

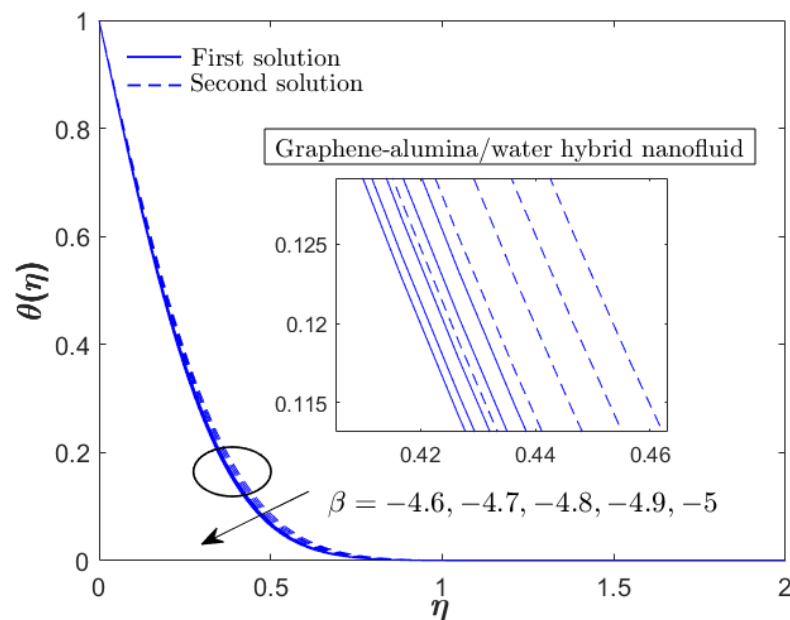


Figure 7. Temperature profile for various β (decelerating parameter) when $\alpha = 1$ and $Z = d = \phi_1 = \phi_2 = 0.01$.

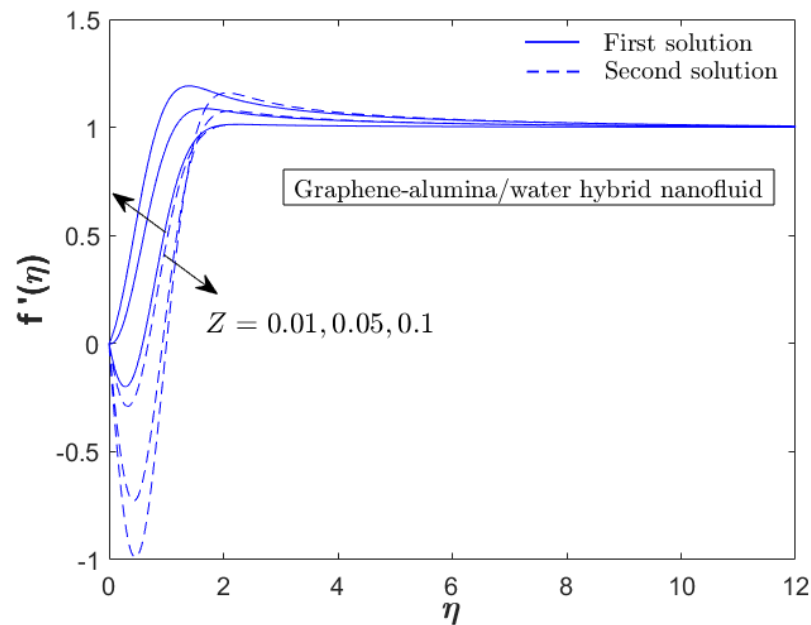


Figure 8. Velocity profile for various Z (EMHD parameter) when $\beta = -5$, $\alpha = 1$ and $d = \phi_1 = \phi_2 = 0.01$.

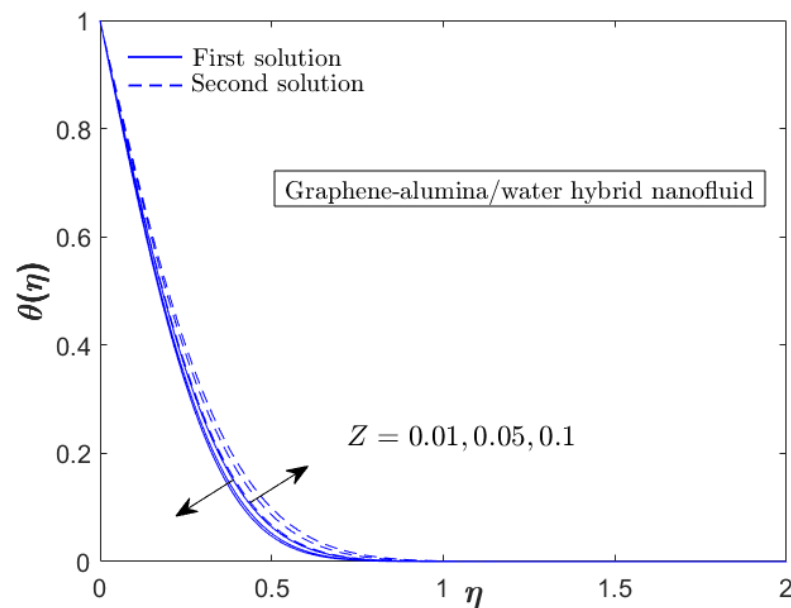


Figure 9. Temperature profile for various Z (EMHD parameter) when $\beta = -5$, $\alpha = 1$ and $d = \phi_1 = \phi_2 = 0.01$.

5. Conclusions

The USSP flow of hybrid nanofluids (copper–alumina/water and graphene–alumina/water) subjected to an EMHD Riga plate is numerically studied. The mathematical model is developed based on few physical and boundary layer assumptions. Similarity transformation is used to reduce the complex model into a set of simpler differential equations which then solved using the bvp4c solver. The main highlight is to analyze and compare the flow and thermal progresses of hybrid nanofluids. The conclusions of the present work are as follows:

- The acceleration parameter enhances the skin friction and heat transfer coefficients for both hybrid nanofluids. However, the graphene–alumina/water has the maximum skin friction coefficient while copper–alumina/water has the maximum thermal coefficient for larger acceleration parameter.

- Upon the comparison of the hybrid and single nanofluids, the graphene–water has the maximum skin friction coefficient while alumina–water has the maximum heat transfer rate followed by graphene–water and copper–water nanofluids. This implies that the single nanofluids are a progressive heat transfer fluid and better than hybrid nanofluids for the case of unsteadiness decelerating flow.
- The increment of the decelerating parameter depreciates the velocity profile while the EMHD parameter accelerates the fluid velocity.
- Both decelerating and EMHD parameters reduce the temperature profile of the hybrid nanofluid by actively transmitting the fluid particle heat.

However, the findings are only conclusive and limited to the comparison between graphene–alumina and copper–alumina with water base fluid. The results may differ if another base fluid is used. Hence, future study is necessary to investigate the thermal progress of these hybrid nanofluids. The recommendations for future study are as follows:

- The researchers can consider oil base fluid like ethylene glycol or combination of water and ethylene glycol.
- The researchers can consider magnetized hybrid nanofluid like magnetite–cobalt ferrite which actively operated under the magnetic field (EMHD) environment.
- The researchers can apply statistical data analysis like response surface methodology (RSM) and sensitivity analysis in investigating the significance of the physical parameters in this physical situation.

Author Contributions: Formulation of mathematical model and methodology, N.S.K., N.M.A. and I.P.; model validation, N.S.K. and N.M.A.; writing, N.S.K. and N.S.W.; review and editing, N.S.K., N.M.A. and N.S.W. All authors have read and agreed to the published version of the manuscript.

Funding: This research received no external funding.

Acknowledgments: We acknowledge the supports from Universiti Putra Malaysia, Universiti Teknikal Malaysia Melaka (FRGS/1/2021/STG06/UTEM/03/1) and Ministry of Higher Education (Malaysia).

Conflicts of Interest: The authors declare no conflict of interest.

References

1. Choi, S.U.S.; Eastman, J.A. Enhancing Thermal Conductivity of Fluids with Nanoparticles. *ASME Fluids Eng. Div.* **1995**, *231*, 99–106.
2. Eastman, J.A.; Choi, S.U.S.; Li, S.; Yu, W.; Thompson, L.J. Anomalous Increased Effective Thermal Conductivities of Ethylene Glycol-Based Nanofluids Containing Copper Nanoparticles. *Appl. Phys. Lett.* **2001**, *78*, 718–720. [[CrossRef](#)]
3. Yu, W.; France, D.M.; Routbort, J.L.; Choi, S.U.S. Review and Comparison of Nanofluid Thermal Conductivity and Heat Transfer Enhancements. *Heat Transf. Eng.* **2008**, *29*, 432–460. [[CrossRef](#)]
4. Yu, W.; Xie, H. A Review on Nanofluids: Preparation, Stability Mechanisms, and Applications. *J. Nanomater.* **2012**, *2012*, 1–17. [[CrossRef](#)]
5. Das, S.K.; Choi, S.U.S.; Patel, H.E. Heat Transfer in Nanofluids—A Review. *Heat Transf. Eng.* **2006**, *27*, 3–19. [[CrossRef](#)]
6. Ali, A.R.I.; Salam, B. A Review on Nanofluid: Preparation, Stability, Thermophysical Properties, Heat Transfer Characteristics and Application. *SN Appl. Sci.* **2020**, *2*, 1636. [[CrossRef](#)]
7. Sidik, N.A.C.; Adamu, I.M.; Jamil, M.M.; Kefayati, G.H.R.; Mamat, R.; Najafi, G. Recent Progress on Hybrid Nanofluids in Heat Transfer Applications: A Comprehensive Review. *Int. Commun. Heat Mass Transf.* **2016**, *78*, 68–79. [[CrossRef](#)]
8. Huminic, G.; Huminic, A. Hybrid Nanofluids for Heat Transfer Applications—A State-of-the-Art Review. *Int. J. Heat Mass Transf.* **2018**, *125*, 82–103. [[CrossRef](#)]
9. Jamil, F.; Ali, H.M. Applications of Hybrid Nanofluids in Different Fields. In *Hybrid Nanofluids for Convection Heat Transfer*; Elsevier: Amsterdam, The Netherlands, 2020; pp. 215–254.
10. Kshirsagar, D.P.; Venkatesh, M.A. A Review on Hybrid Nanofluids for Engineering Applications. *Mater. Today Proc.* **2021**, *44*, 744–755. [[CrossRef](#)]
11. Vallejo, J.P.; Prado, J.I.; Lugo, L. Hybrid or Mono Nanofluids for Convective Heat Transfer Applications. A Critical Review of Experimental Research. *Appl. Therm. Eng.* **2022**, *203*, 117926. [[CrossRef](#)]
12. Suresh, S.; Venkitaraj, K.P.; Selvakumar, P.; Chandrasekar, M. Effect of Al₂O₃–Cu/Water Hybrid Nanofluid in Heat Transfer. *Exp. Therm. Fluid Sci.* **2012**, *38*, 54–60. [[CrossRef](#)]

13. Madhesh, D.; Kalaiselvam, S. Experimental Analysis of Hybrid Nanofluid as a Coolant. *Procedia Eng.* **2014**, *97*, 1667–1675. [[CrossRef](#)]
14. Alawi, O.A.; Kamar, H.M.; Hussein, O.A.; Mallah, A.R.; Mohammed, H.A.; Khiadani, M.; Roomi, A.B.; Kazi, S.N.; Yaseen, Z.M. Effects of Binary Hybrid Nanofluid on Heat Transfer and Fluid Flow in a Triangular-Corrugated Channel: An Experimental and Numerical Study. *Powder Tech.* **2022**, *395*, 267–279. [[CrossRef](#)]
15. Gailitis, A.; Lielausis, O. On a Possibility to Reduce the Hydrodynamic Resistance of a Plate in an Electrolyte. *Appl. Magneto-hydrodyn.* **1961**, *12*, 143–146.
16. Ganesh, N.V.; Al-Mdallal, Q.M.; Al Fahel, S.; Dadoa, S. Riga–Plate Flow of γ Al₂O₃-Water/Ethylene Glycol with Effective Prandtl Number Impacts. *Heliyon* **2019**, *5*, e01651. [[CrossRef](#)]
17. Hayat, T.; Abbas, T.; Ayub, M.; Farooq, M.; Alsaedi, A. Flow of Nanofluid Due to Convectively Heated Riga Plate with Variable Thickness. *J. Mol. Liq.* **2016**, *222*, 854–862. [[CrossRef](#)]
18. Ayub, M.; Abbas, T.; Bhatti, M.M. Inspiration of Slip Effects on Electromagnetohydrodynamics (EMHD) Nanofluid Flow through a Horizontal Riga Plate. *Eur. Phys. J. Plus* **2016**, *131*, 193. [[CrossRef](#)]
19. Ramzan, M.; Bilal, M.; Chung, J.D. Radiative Williamson Nanofluid Flow over a Convectively Heated Riga Plate with Chemical Reaction-A Numerical Approach. *Chin. J. Phys.* **2017**, *55*, 1663–1673. [[CrossRef](#)]
20. Zari, I.; Ali, F.; Khan, T.S.; Shafiq, A. Radiative Hiemenz flow towards a stretching Riga plate in hybrid nanofluid. *Int. Comm. Heat Mass Transf.* **2022**, *139*, 106492. [[CrossRef](#)]
21. Abbas, N.; Nadeem, S.; Malik, M.Y. Theoretical Study of Micropolar Hybrid Nanofluid over Riga Channel with Slip Conditions. *Phys. A* **2020**, *551*, 124083. [[CrossRef](#)]
22. Khashi'ie, N.S.; Waini, I.; Kasim, A.R.M.; Zainal, N.A.; Arifin, N.M.; Pop, I. Thermal Progress of a Non-Newtonian Hybrid Nanofluid Flow on a Permeable Riga Plate with Temporal Stability Analysis. *Chin. J. Phys.* **2022**, *77*, 279–290. [[CrossRef](#)]
23. Khashi'ie, N.S.; Waini, I.; Arifin, N.M.; Pop, I. Dual solutions of unsteady two-dimensional electro-magneto-hydrodynamics (EMHD) axisymmetric stagnation-point flow of a hybrid nanofluid past a radially stretching/shrinking Riga surface with radiation effect. *Int. J. Numer. Methods Heat Fluid Flow* **2022**, *33*, 333–350. [[CrossRef](#)]
24. Khashi'ie, N.S.; Zokri, S.M.; Kasim, A.R.M.; Waini, I.; Zainal, N.A. Insight into hybrid nanofluid induced by a Riga plate: Investigation on second grade fluid model. *Waves Random Complex Media* **2022**. [[CrossRef](#)]
25. Zainal, N.A.; Nazar, R.; Naganthran, K.; Pop, I. Unsteady Stagnation Point Flow Past a Permeable Stretching/Shrinking Riga Plate in Al₂O₃-Cu/H₂O Hybrid Nanofluid with Thermal Radiation. *Int. J. Numer. Methods Heat Fluid Flow* **2022**, *32*, 2640–2658. [[CrossRef](#)]
26. Wahid, N.S.; Arifin, N.M.; Khashi'ie, N.S.; Pop, I.; Bachok, N.; Hafidzuddin, M.E.H. Hybrid Nanofluid Stagnation Point Flow Past a Slip Shrinking Riga Plate. *Chin. J. Phys.* **2022**, *78*, 180–193. [[CrossRef](#)]
27. Tabassum, R.; Al-Zubaidi, A.; Rana, S.; Mehmood, R.; Saleem, S. Slanting transport of hybrid (MWCNTs-SWCNTs/H₂O) nanofluid upon a Riga plate with temperature dependent viscosity and thermal jump condition. *Int. Comm. Heat Mass Transf.* **2022**, *135*, 106165. [[CrossRef](#)]
28. Shatnawi, T.A.; Abbas, N.; Shatanawi, W. Mathematical Analysis of Unsteady Stagnation Point Flow of Radiative Casson Hybrid Nanofluid Flow over a Vertical Riga Sheet. *Mathematics* **2022**, *10*, 3573. [[CrossRef](#)]
29. Siddique, I.; Khan, Y.; Nadeem, M.; Awrejcewicz, J.; Bilal, M. Significance of heat transfer for second-grade fuzzy hybrid nanofluid flow over a stretching/shrinking Riga wedge. *AIMS Math.* **2023**, *8*, 295–316. [[CrossRef](#)]
30. Kumar, L. Cu–Al₂O₃/engine oil Williamson hybrid nanofluid flow over a stretching/shrinking Riga plate with viscous dissipation and radiation effect. *Heat Transf.* **2022**, *51*, 2279–2305. [[CrossRef](#)]
31. Asogwa, K.K.; Mebarek-Oudina, F.; Animasaun, I.L. Comparative investigation of water-based Al₂O₃ nanoparticles through water-based CuO nanoparticles over an exponentially accelerated radiative Riga plate surface via heat transport. *Arab. J. Sci. Eng.* **2022**, *47*, 8721–8738. [[CrossRef](#)]
32. Ma, P.K.H.; Hui, W.H. Similarity Solutions of the Two-Dimensional Unsteady Boundary-Layer Equations. *J. Fluid Mech.* **1990**, *216*, 537–559. [[CrossRef](#)]
33. Dholey, S.; Gupta, A.S. Unsteady Separated Stagnation-Point Flow of an Incompressible Viscous Fluid on the Surface of a Moving Porous Plate. *Phys. Fluids* **2013**, *25*, 023601. [[CrossRef](#)]
34. Dholey, S. Unsteady Separated Stagnation-Point Flow over a Permeable Surface. *Z. Angew. Math. Phys.* **2019**, *70*, 10. [[CrossRef](#)]
35. Lok, Y.Y.; Pop, I. Stretching or Shrinking Sheet Problem for Unsteady Separated Stagnation-Point Flow. *Meccanica* **2014**, *49*, 1479–1492. [[CrossRef](#)]
36. Dholey, S. Magnetohydrodynamic Unsteady Separated Stagnation-Point Flow of a Viscous Fluid over a Moving Plate. *Z. Angew. Math. Mech.* **2016**, *96*, 707–720. [[CrossRef](#)]
37. Dholey, S. An Unsteady Separated Stagnation-Point Flow Towards a Rigid Flat Plate. *J. Fluids Eng.* **2019**, *141*, 021202. [[CrossRef](#)]
38. Dholey, S. Unsteady Separated Stagnation-Point Flows and Heat Transfer over a Plane Surface Moving Normal to the Flow Impingement. *Int. J. Therm. Sci.* **2021**, *163*, 106688. [[CrossRef](#)]
39. Roşca, N.C.; Roşca, A.V.; Pop, I. Unsteady Separated Stagnation-Point Flow and Heat Transfer Past a Stretching/Shrinking Sheet in a Copper-Water Nanofluid. *Int. J. Numer. Methods Heat Fluid Flow* **2019**, *29*, 2588–2605. [[CrossRef](#)]
40. Renuka, A.; Muthamilselvan, M.; Al-Mdallal, Q.M.; Doh, D.H.; Abdalla, B. Unsteady Separated Stagnation Point Flow of Nanofluid Past a Moving Flat Surface in the Presence of Buongiorno's Model. *J. Appl. Comp. Mech.* **2021**, *7*, 1283–1290. [[CrossRef](#)]

41. Khashi'ie, N.S.; Wahid, N.S.; Arifin, N.M.; Pop, I. Magneto hydrodynamics Unsteady Separated Stagnation-point (USSP) Flow of a Hybrid Nanofluid on a Moving Plate. *Z. Angew. Math. Mech.* **2022**, *102*, e202100410. [[CrossRef](#)]
42. Zainal, N.A.; Nazar, R.; Naganthran, K.; Pop, I. Magnetic Impact on the Unsteady Separated Stagnation-Point Flow of Hybrid Nanofluid with Viscous Dissipation and Joule Heating. *Mathematics* **2022**, *10*, 2356. [[CrossRef](#)]
43. Khashi'ie, N.S.; Waini, I.; Wahid, N.S.; Arifin, N.M.; Pop, I. Unsteady separated stagnation point flow due to an EMHD Riga plate with heat generation in hybrid nanofluid. *Chin. J. Phys.* **2022**, *81*, 181–192. [[CrossRef](#)]
44. Takabi, B.; Salehi, S. Augmentation of the Heat Transfer Performance of a Sinusoidal Corrugated Enclosure by Employing Hybrid Nanofluid. *Adv. Mech. Eng.* **2015**, *6*, 147059. [[CrossRef](#)]
45. Sparrow, E.M.; Yu, H.S. Local non-similarity thermal boundary-layer solutions. *J. Heat Transf.* **1971**, *93*, 328–334. [[CrossRef](#)]
46. Hussain, M.; Sheremet, M. Convection analysis of the radiative nanofluid flow through porous media over a stretching surface with inclined magnetic field. *Int. Commun. Heat Mass Transf.* **2023**, *140*, 106559. [[CrossRef](#)]
47. Kumar, R.; Kumar, S.; Gourla, M.G. Axi-symmetric deformation due to various sources in saturated porous media with incompressible fluid. *J. Solid Mech.* **2013**, *5*, 74–91.
48. Abbas, I.A. Eigenvalue approach on fractional order theory of thermoelastic diffusion problem for an infinite elastic medium with a spherical cavity. *Appl. Math. Model.* **2015**, *39*, 6196–6206. [[CrossRef](#)]
49. Merkin, J.H. On Dual Solutions Occurring in Mixed Convection in a Porous Medium. *J. Eng. Math.* **1986**, *20*, 171–179. [[CrossRef](#)]
50. Weidman, P.D.; Kubitschek, D.G.; Davis, A.M.J. The Effect of Transpiration on Self-Similar Boundary Layer Flow over Moving Surfaces. *Int. J. Eng. Sci.* **2006**, *44*, 730–737. [[CrossRef](#)]
51. Harris, S.D.; Ingham, D.B.; Pop, I. Mixed Convection Boundary-Layer Flow Near the Stagnation Point on a Vertical Surface in a Porous Medium: Brinkman Model with Slip. *Transp. Porous Med.* **2009**, *77*, 267–285. [[CrossRef](#)]
52. Ahmad, R.; Mustafa, M.; Turkyilmazoglu, M. Buoyancy effects on nanofluid flow past a convectively heated vertical Riga-plate: A numerical study. *Int. J. Heat Mass Transf.* **2017**, *111*, 827–835. [[CrossRef](#)]
53. Ahammed, N.; Asirvatham, L.G.; Wongwises, S. Entropy generation analysis of graphene–alumina hybrid nanofluid in multiport minichannel heat exchanger coupled with thermoelectric cooler. *Int. J. Heat Mass Transf.* **2016**, *103*, 1084–1097. [[CrossRef](#)]

Disclaimer/Publisher's Note: The statements, opinions and data contained in all publications are solely those of the individual author(s) and contributor(s) and not of MDPI and/or the editor(s). MDPI and/or the editor(s) disclaim responsibility for any injury to people or property resulting from any ideas, methods, instructions or products referred to in the content.